applied optics

Model-based analysis on the influence of spatial frequency selection in spatial frequency domain imaging

Nico Bodenschatz,* Philipp Krauter, André Liemert, Joachim Wiest, and Alwin Kienle

Institut für Lasertechnologien in der Medizin und Meßtechnik, Helmholtzstr. 12, D-89081 Ulm, Germany
**Corresponding author: nico.bodenschatz@uni-ulm.de*

Received 21 April 2015; revised 27 June 2015; accepted 2 July 2015; posted 6 July 2015 (Doc. ID 238558); published 24 July 2015

Frequency variation in spatial frequency domain imaging is a powerful tool for adjusting the penetration depth of the imaging signal and the parameter sensitivity toward absorption and diffusive and subdiffusive scattering. Through our computational analysis, using an analytical solution of the radiative transfer equation, we add quantitation to this tool by linking the different spatial frequency regimes to their relative information content and to their absolute depth sensitivity. Special focus is placed on high spatial frequencies by analysis of the phase function parameter γ and its significance and ambiguity in describing subdiffusive scattering.

OCIS codes: (290.7050) Turbid media; (170.3660) Light propagation in tissues; (290.5825) Scattering theory; (170.7050) Turbid media.

http://dx.doi.org/10.1364/AO.54.006725

1. INTRODUCTION

Spatial frequency domain imaging (SFDI) is a diffuse optical imaging modality that is frequently used to derive absorption and scattering maps of turbid media [1–8]. Its great advantage over other techniques is the spatial resolution of the derived optical properties. The technique employs spatially modulated sinusoidal light-intensity projections and uses the diffusely backscattered light to derive optical properties using a suitable light propagation model [3,9,10]. Therefore, the spatial frequency of the projection pattern has implications on the depth sensitivity [1] and on the sensitivity toward absorption and scattering.

The typical spatial frequency range for mapping of absorption and scattering in tissue is on the low-frequency end in order to maximize the absorption contrast and to achieve maximum depth sensitivity. At the same time, the measurement at multiple frequencies is a prerequisite to separate absorption and scattering in the diffuse reflectance signal. While there seems to be an established frequency regime in SFDI, the best spatial frequency choice, depending on the sought-after optical parameters, is somewhat unknown. Therefore, we analyzed the depth sensitivity and the relative information content of spatial frequency domain (SFD) reflectance with respect to absorption, scattering, and the scattering phase function for a large range of spatial frequencies. By setting the focus to high spatial frequencies, we continued from our previous work to further investigate the influence of the scattering phase function in SFDI [11].

All our studies are based on optical property ranges typical for human or animal tissue [12–14]. In the first part of this work (Section 2), we examine the theoretical relationship between different spatial frequency values and their corresponding sensitivity to the absorption, scattering, and scattering phase function parameters, respectively. This allows for identification of ideal frequency values for the extraction of absorption and scattering parameters in turbid media. Additionally, we relate spatial frequency values to their corresponding depth sensitivity and provide depth sensitivity maps in dependence of the optical properties.

In Section 3, we focus on high spatial frequencies and investigate the extent to which structural information of scatterers possibly can be detected using nonpolarized SFDI. To this end, we studied the significance of the phase function parameter γ and made theoretical investigations on its information content. By comparison of different phase functions, we were able to reveal ambiguity in the inverse problem, when trying to extract γ from experimental SFDI data. Based on this analysis, we suggest possible strategies that minimize the uncertainty in the derivation of γ for biological tissue.

2. SENSITIVITY REGIMES IN SFDI

In view of its biomedical application, experimentalists typically aim for the absorption coefficient μ_a and the reduced scattering coefficient μ_s' when performing SFDI. Therefore, μ_a can carry

valuable information about metabolic properties such as perfusion, oxygenation, and chemical content and μ_s' is related to structural tissue properties like cell density or tissue type [3,7].

In most SFDI studies, spatial frequencies below $f = 0.3\ \mathrm{mm}^{-1}$ (corresponding to $k \approx 1.9\,\frac{\mathrm{rad}}{\mathrm{mm}}$) are used. While this regime has become a best practice, the implications of expanding or reducing the frequency range are typically not considered.

In contrast with other diffuse optical imaging technologies such as spatially resolved reflectance, subdiffusive light is always part of the SFD reflectance signal due to its wide-area projection [15]. The relative influence of subdiffusive light on SFD reflectance is strongly dependent on the spatial frequency and may be diminished or enhanced by proper selection of the spatial frequency range [16]. Subdiffusive light propagation is characterized by the underlying scattering phase function and has been found to be well quantified by the phase function parameter $\gamma = \frac{1-g_2}{1-g_1}$, where g_1 and g_2 are the first- and second-order Legendre moments of the scattering phase function, respectively [17,18]. In the following, we use this parameter to quantify the sensitivity toward subdiffusive light propagation in SFDI. Therefore, we make frequent use of the term "SFD reflectance" or simply "reflectance" and refer to the demodulated amplitude (AC reflectance signal), which is typically obtained from three successively captured phase images [1].

We quantify the parameter sensitivity of SFD reflectance by calculation of derivatives with respect to the different optical parameters. Our analysis is based on an analytical solution of the radiative transfer equation (RTE) for spatially modulated projections on semi-infinite, homogeneous, and isotropic scattering media [19,20]. Using this model, we calculated a large set of SFD reflectance data R for a broad range of biologically relevant optical parameters [12,13], namely, $0.003\ \mathrm{mm}^{-1} \le \mu_a \le 0.3\ \mathrm{mm}^{-1}$ and $0.3\ \mathrm{mm}^{-1} \le \mu_s' \le 3\ \mathrm{mm}^{-1}$. A simulation grid of 10×10 within these parameter ranges was formed, and the derivative of R with respect to μ_a and μ_s' was calculated and expressed in terms of scaled spatial frequencies f/μ_s' at every grid point. By normalizing and subsequently averaging the derivatives of all grid points, two curves with respect to μ_a and μ_s' were obtained. We show these curves in Fig. 1, illustrating the sensitivity of SFDI toward absorption and scattering.

In previous studies, fractal size distributions of scatterers were found to agree well with the angular scattering characteristics of cells [21–25] and are able to reproduce the observed nature of refractive index fluctuations in tissue [26]. Therefore, we base our sensitivity analysis on this fractal phase function type with a fractal dimension of $\alpha = 4.4$ corresponding to $\gamma = 1.8$. This γ value corresponds to the mean of reported *in vivo* studies on γ for various tissue types [27–29]. The fractal phase function assumes a weighted average of Mie scatterers with the number concentration ρ following the power law

$$\rho(d) = Ad^{-\alpha}, \tag{1}$$

with scaling factor A [14]. In our case, the wavelength was set to $\lambda = 600$ nm, and we used 500 discrete Mie scatterers with a diameter between $d = 1$ nm and $d = 10$ μm to approximate the power law. The refractive indices were set to $n_i = 1.40$ and $n_o = 1.33$ inside and outside the scatterers, respectively [25].

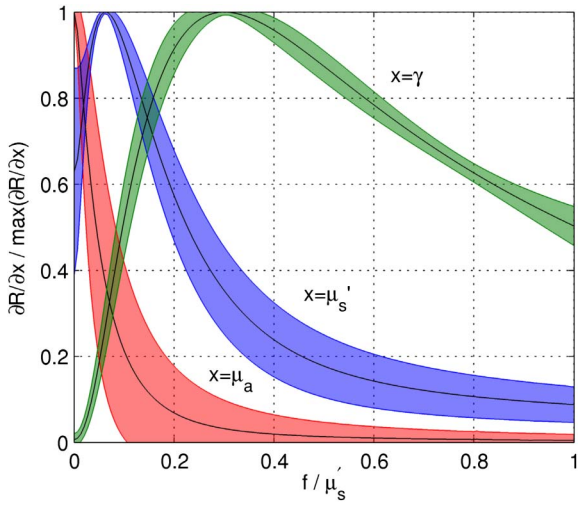

Fig. 1. Normalized sensitivity of SFD reflectance toward the different optical parameters x (μ_a, μ_s', and γ) for different scaled spatial frequencies. Every curve stands for an average of the respective derivative $\partial R/\partial x$ computed for a large set of optical properties. The shaded areas give the standard deviation of the corresponding average.

In order to also study the sensitivity toward γ, a similar calculation was carried out using a series of γ values representing the measured and anticipated γ range for human tissue. To this end, the SFD reflectance for 100 different fractal scattering phase functions was calculated with fractal dimensions linearly spaced between $3.3 \le \alpha \le 5.5$ (corresponding to $1.3 \le \gamma \le 2.4$) using the same particle sizes and refractive indices as above. In the next step, the derivative of R was formed with respect to γ for all 100 reflectance curves and averaged to yield the third normalized curve, as shown in Fig. 1. Due to the small dependence of μ_a and μ_s' on $\partial R/\partial\gamma$, the absorption and reduced scattering value were fixed to $\mu_a = 0.01\ \mathrm{mm}^{-1}$ and $\mu_s' = 1\ \mathrm{mm}^{-1}$, respectively.

From the three curves in Fig. 1, the relative importance of μ_a, μ_s', and γ at different spatial frequency regimes can be understood. Accordingly, the strongest influence of μ_a on the SFD reflectance exists at the low-frequency end and diminishes quickly for higher frequencies. The influence of μ_s' is found to be maximal at about $f/\mu_s' = 0.06$ but also affects reflectance at low and very high spatial frequencies. The maximum relative influence of γ on the reflectance curve is found at $f/\mu_s' \approx 0.31$ and maintains its prominence also for higher frequencies. Noticeably, its influence reduces strongly toward the low-frequency end, and a small influence remains even at spatial frequency zero [16]. All our computations are based on the numerical detection aperture NA = 1, and it should be considered that low spatial frequencies are much more sensitive to γ for lower detection apertures based on the distinct angular reflectance characteristics of subdiffusive scattering.

Based on the large set of optical properties considered, it is not possible to generally compare the derivative curves on an absolute scale without normalization. One should, however, be aware that the absolute influence of μ_s' may well exceed that of μ_a or γ at the low- or high-frequency end, respectively. As an example, the derivatives $\partial R/\partial\mu_s'$ and $\partial R/\partial\gamma$ are almost the same

on an absolute scale at $f/\mu_s' = 0.31$ mm^{-1} for $\mu_a = 0.01$ mm^{-1}, $\mu_s' = 1$ mm^{-1} and $\gamma = 1.8$. One should therefore not underestimate the influence of μ_s' at high spatial frequencies based on Fig. 1.

Every curve in Fig. 1 represents an average value and is therefore embedded in a shaded area, thus giving the standard deviation of the corresponding averaging. Note that the graph's y axis is limited to values between 0 and 1 and does not fully depict the symmetry of the standard deviations with respect to the curves.

In spite of its normalized values, Fig. 1 offers several important findings. First, there is no frequency range where any of the three parameters μ_a, μ_s', and γ can be derived without consideration of a second parameter.

Second, it can be observed that the parasitic influence of the scattering phase function on the measurement of μ_a and μ_s' can be diminished by limitation of the frequency range to about $f/\mu_s' \leq 0.1$, without losing too much information on μ_s'. One should keep in mind that a model-based wrong assumption in γ of only $\Delta\gamma = 0.2$ can already cause a 10% error in μ_s' when using the frequency range $0 \leq f/\mu_s' \leq 0.2$ [11].

Third, it may be possible for sufficiently small absorption values to disregard the influence of μ_a and to measure μ_s' and γ by considering only high spatial frequencies.

In the next step, we want to relate the different spatial frequency regimes to their corresponding propagation depths and give an example of the typical number of scattering interactions involved. In Fig. 2, we show the SFD reflectance as predicted from Monte Carlo simulations for semi-infinite media with $\mu_a = 0.01$ mm^{-1}, $\mu_s' = 1$ mm^{-1}, and fractal scattering using $\alpha = 4.4$ (all other parameters as above). In addition to the actual SFD reflectance curve for these parameters (solid line), we also show the simulated spatial frequency reflectance as obtained by limiting the number of maximum scattering interactions to 1, 5, 10, 50, and 100, respectively (dashed curves). Accordingly, while the actual reflectance signal can only be obtained by allowing a very large number of interactions (in this case 1000 or more), a limited number of interactions suffice to produce the correct reflectance signal at high frequencies. The actual number of required interactions is mostly dependent on the first Legendre moment g_1 of the scattering phase function.

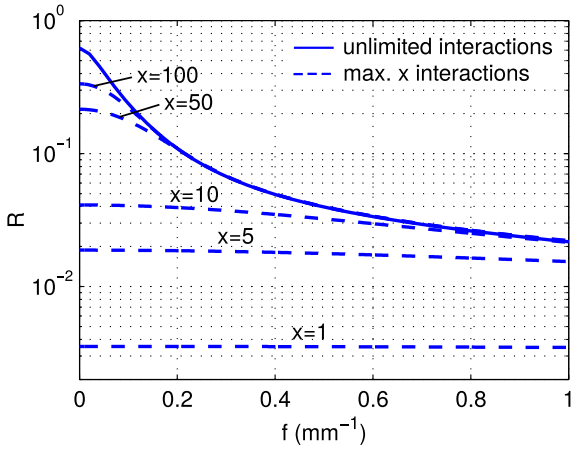

Fig. 2. Spatial frequency domain (SFD) reflectance as predicted by a Monte Carlo simulation for $\mu_a = 0.01$ mm^{-1}, $\mu_s' = 1$ mm^{-1}, and $g_1 = 0.91$ (solid curve). The dashed curves correspond with the same simulation with limitation of the allowed number of scattering interactions to a maximum of 1, 5, 10, 50, or 100 interactions.

The lowest dashed curve in Fig. 2 corresponds to only a single scattering interaction. This curve is almost a horizontal line across all frequencies. Consequently, subdiffusive or ballistic photons contribute nearly equally at all spatial frequencies. By gradually increasing the number of maximum interactions, one finds that photons are decreasingly likely to contribute to high spatial frequency reflectance. In this case, photons with more than 50 scattering interactions have negligible contribution for frequencies above $f = 0.3$ mm^{-1}. This is because an increasing number of scattering interactions corresponds on average to a larger propagation distance and, thus, to a decline in high-frequency content.

The considerations in Fig. 2 have three useful implications. First, small volumes of turbid media suffice to perform measurements at high spatial frequencies, where deeply penetrating light no longer contributes to the reflectance signal. Second, Monte Carlo simulations for modeling of subdiffusive light propagation may be accelerated by about an order of magnitude through limiting the number of scattering interactions. Third, the reflectance at very high spatial frequencies may be subtracted from that of low spatial frequencies to reduce the qualitative influence of specular reflections from rough surfaces without using polarization filters [16]. This subtraction may reduce the image noise related to surface effects and, thus, enhance the visibility of deep tissue heterogeneities. However, even though this procedure also eliminates specular reflections from SFDI data, it cannot reduce the potential error in μ_a and μ_s' due to uncertainty in the scattering phase function.

In order to understand the penetration depth of light that contributes at a certain spatial frequency, we present the average and the near maximal penetration depth computed for a large set of optical properties in Figs. 3 and 4, respectively. Using a recently discovered analytical solution to the RTE for layered media (to be published, and based on the approach of Liemert and Kienle [19,20]) assuming normal incidence of a spatially modulated light source, we applied the following procedure to investigate the penetration depth of light [30,31]. In the model, we assumed a two layered media and set the optical properties of the bottom layer such that light entering the second layer is always absorbed and has no chance to be reflected back to the first layer. In the first layer, we chose a set of optical properties and assumed fractal scattering with $\alpha = 4.4$ as above. In an iterative computation, we determined the thickness d_x of the first layer such that the absolute diminishing impact of the black bottom layer on the SFD reflectance signal is exactly $x = 50\%$ or $x = 5\%$. These depths serve as an approximation to the average and near maximal penetration depths of light, and we show their values dependent on spatial frequency and for a large set of first layer optical properties in Figs. 3 and 4, respectively.

Figures 3 and 4 were computed for a fixed value of $\mu_s' = 1$ mm^{-1} but are also transferable to other reduced scattering values by consideration of the scaled spatial frequency f/μ_s' and the scaled depth $d_x\mu_s'$. As an example, for $\mu_a = 0.01$ mm^{-1}

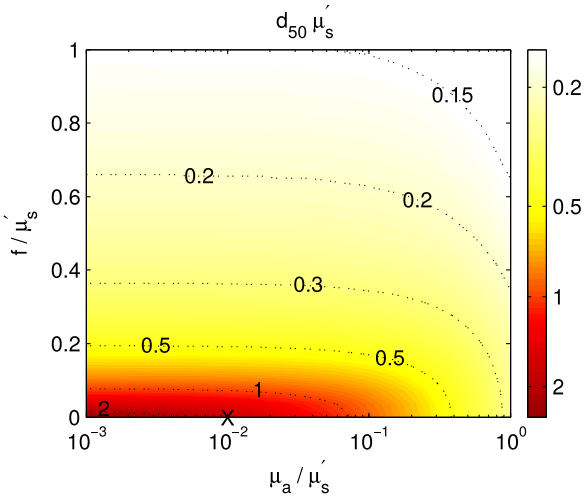

Fig. 3. Look-up graphic for the average scaled penetration depth $d_{50}\mu_s'$ for a large range of optical properties and scaled spatial frequencies.

and $\mu_s' = 1\ \text{mm}^{-1}$, we find $d_{50} = 1.8$ mm and $d_5 = 7.7$ mm at spatial frequency zero (both values are marked by a cross in Figs. 3 and 4). Note that the influence on the reflectance of a second layer at depth d_5 (or d_{50}) can actually be larger than 5 (or 50) percent, if the scattering of this second layer exceeds that of the upper layer.

3. HIGH SPATIAL FREQUENCY ANALYSIS

According to Section 2, the high spatial frequency regime is characterized by a very low sensitivity to μ_a, a maintained sensitivity to μ_s', and an increasing influence of subdiffusive scattering. The scattering anisotropy $g_1 = \langle\cos(\theta)\rangle$, which is defined as the mean cosine of the scattering angle θ, has often been considered as the key parameter in the subdiffusive regime [21,32]. However, as demonstrated by Bevilacqua and Depeursinge in 1999 [18], subdiffusive backscattering strongly depends on the first and second Legendre moment of the phase function and is well quantified by the dimensionless parameter $\gamma = \frac{1-g_2}{1-g_1}$. In spite of its counterintuitive mathematical definition, γ has been found to correlate almost linearly with the fractal dimension of turbid media in the anticipated biological scattering regime [14]. In general terms, γ inversely quantifies the subdiffusive backscattering efficiency. Small γ values correspond to large reflectance in proximity to the source and, thus, at high spatial frequencies.

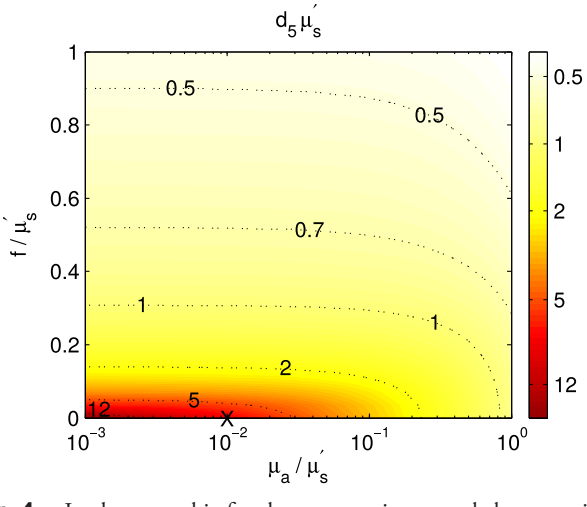

Fig. 4. Look-up graphic for the near maximum scaled penetration depth $d_5\mu_s'$ for a large range of optical properties and scaled spatial frequencies.

When investigating single Mie scatterers of diameter d, it can be found that a relation between the scaled size parameter d/λ and γ exists. This relation is dependent on the refractive index ratio $m = n_i/n_o$ of the inside and outside of the scattering particle and may be studied experimentally by measuring γ for monosized particles over a broad wavelength range. In our case, the relations were found by numerical computation and are given in Fig. 5 for various refractive index ratios.

For the typical situation, where no additional information on the measured scattering particles is available, the low- and high-frequency oscillations shown in the curves of Fig. 5 demonstrate an ambiguity in trying to relate a particular γ value to the size of scattering particles. This ambiguity is very pronounced for particles with a high refractive index mismatch, as can be seen by the decline of the lower curves in Fig. 5 at larger particle sizes. In spite of these ambiguities, γ still demonstrates a meaningful parameter for quantification of the size characteristics of biological tissue based on two reasons. On the one hand, the typical amplitude Δn of refractive index variations in biological tissue tends to be small (typically $\Delta n < 0.1$) [25,26,33,34], thereby avoiding the low-frequency oscillations in Fig. 5. On the other hand, biological tissue contains a broad distribution of scattering particles, which evens out the ambiguity related to the high-frequency oscillations [26].

As a single parameter, γ cannot contain the entire complexity of the scattering phase function and, thus, higher-order Legendre moments are required to fully quantify subdiffusive scattering. The potential impact of these higher-order Legendre moments is frequently disregarded when performing measurements to retrieve γ. The common approach toward measuring γ is to assume a simplified scattering phase function within a light propagation model and to fit this model to the reflectance data

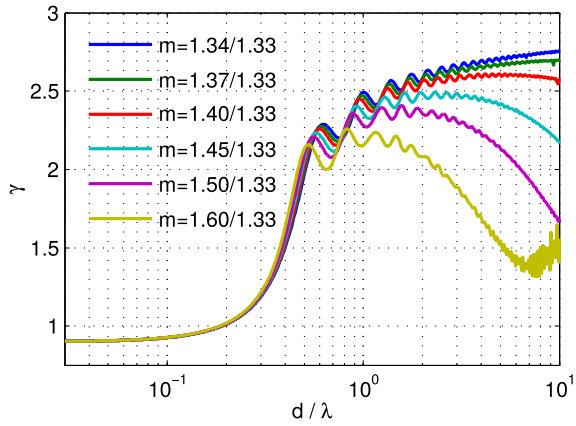

Fig. 5. Computed γ values for single Mie scatterers of different size parameter d/λ and different refractive index ratios m.

using a series of forward calculations [14,28,35,36]. By choosing a specific model phase function type, its general shape characteristics in angular and Legendre space are determined. Consequently, when comparing the reflectance of different phase function types at fixed γ values, the influence of higher-order Legendre moments becomes apparent.

We employed a series of five different scattering phase function types for the simulation of SFD reflectance at the fixed scaled spatial frequency of $f/\mu_s' = 0.31$. This frequency value is selected because of its maximum sensitivity toward γ (see Fig. 1). Figure 6 shows the calculated reflectance values at this single frequency versus γ with the absorption and scattering value fixed to $\mu_a = 0.01\ \text{mm}^{-1}$ and $\mu_s' = 1\ \text{mm}^{-1}$, respectively. The five selected phase function types are represented by different colors or shading. The solid black curve corresponds to the previously considered fractal distribution of Mie scatterers (see Section 2), and the dashed black curve represents a Gaussian distribution of Mie scatterers with standard deviation $\sigma_d = 0.25d$ and refractive index ratio $m = 1.40/1.33$. The three shaded areas represent the reflectance ranges accessible by the Reynolds–McCormick scattering phase function (R-McC, with $-0.5 \le \alpha \le 5$ and $|g| \le 1$ as defined by Reynolds and McCormick [37]), the modified Henyey–Greenstein function [18] (MHG, with $|g_{\text{HG}}| < 1$ and $0 \le \alpha \le 1$) and the modified powers of cosines function (MPC, with $0 \le \alpha \le 1$ and $0 \le N \le 100$ as defined by Bevilacqua and Depeursinge [18]).

Figure 6 contains essential information for the accurate measurement of γ. In what is often called the inverse problem, one finds oneself confronted with reflectance data and seeks to derive optical properties from it by using an appropriate light propagation model. In this context, Fig. 6 provides the conclusion that a single reflectance value such as $R(f/\mu_s' = 0.31) = 0.08$ cannot be uniquely mapped to a particular γ value. Instead, using different phase function types, a large range of γ values can lead to the same reflectance value. In this example, using different parameters for the MPC phase function, the reflectance value $R = 0.08$ could correspond to any γ value between 1.2 and 1.8. Consequently, if no specifics about the actual phase function of a sample are known, this range in γ also represents the possible error and the potential influence of higher-order Legendre moments. This source of error may also be a cause of recently reported deviations between measured and expected γ values [14,28].

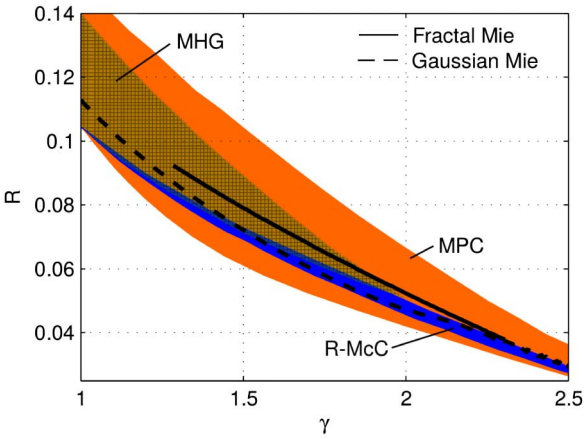

Fig. 6. Spatial frequency domain reflectance at the fixed frequency of $f/\mu_s' = 0.31$ with constant absorption and scattering intensity for a large set of different scattering phase functions. The shaded areas correspond to the large variability that relates to the choice of the different scattering phase functions and illustrates the ambiguity in the derivation of γ.

To minimize the potential error of γ measurements, the appropriateness of the employed model phase function must be ensured. Several studies suggest that a fractal distribution of Mie scatterers may serve as a reasonable approximation to cell and tissue scattering [14,21–26]. In view of long computation times and required high computation orders for corresponding radiative transfer models, the variable yet simpler MPC function may also be used to approximate a fractal distribution of Mie scatterers. Based on Fig. 6, we found the empirical formula,

$$\alpha(N) = \frac{p_1 N^2 + p_2 N + p_3}{N^2 + q_1 N + q_2}, \tag{2}$$

relating the two input parameters of the MPC function for best emulation of fractal scattering. A similar best fit is found for the SFD reflectance values of the Gaussian distribution in Fig. 6, and the corresponding parameters are given in Table 1.

According to Fig. 6, neither the RMcC nor the MHG function can fully reproduce the γ reflectance relationship of fractal or Gaussian–Mie scattering, as they are either limited in their γ range and/or in their variability in higher-order Legendre moments.

It is a great feature of fractal scattering that its γ reflectance characteristic is almost independent of the refractive index ratio m and, thus, unaffected by the uncertainty in the amplitude of refractive index fluctuations in tissue. The same does not apply for a Gaussian distribution of Mie scatterers for large refractive index ratios $m \ge 1.1$, where the γ reflectance relation is non-bijective and does no longer allow for unique γ matching. The use of a narrow size distribution of high refractive index scatterers for precise experimental quantification of γ is therefore inappropriate.

The data of Fig. 6 has been calculated for a fixed spatial frequency and by integrating the reflectance over the entire detection half-sphere (NA = 1). We also performed similar calculations at $f/\mu_s' = 0.1$ and $f/\mu_s' = 1$ and obtained relations that are similar to those shown in Fig. 6 yet weaker in their absolute dependency on γ. Our conclusions based on the fixed frequency analysis are therefore valid over a very large spatial frequency range. Furthermore, computations were also performed for smaller detection apertures, and we found that the associated reduction in reflectance intensity depends to some extend on the phase function type. Indeed, we observed

Table 1. Empirical Parameters for Eq. (2) Relating the Two Input Parameters of the MPC Phase Function for Best Imitation of Fractal or Gaussian Scattering

	p_1	p_2	p_3	q_1	q_2
Fractal	1.026	1.14	3.28	1.40	5.53
Gaussian	0.987	−0.674	1.04	−0.682	1.44

that our empirical relations based on Eq. (2) and Table 1 are only partially valid for smaller detection angles and may allow for errors in γ of up to about 0.1 for numerical detection apertures of NA $\leq$ 0.35 and less. This leads to the additional conclusion that also the detection aperture may have major influence on the quantification of γ and requires proper modeling.

4. CONCLUSION

The variation of spatial frequencies in SFDI is a powerful tool to adjust the relative sensitivity toward absorption and diffusive and subdiffusive scattering. By systematic modeling of tissue optical properties, we were able to distinguish absolute spatial frequency regimes with respect to their parameter sensitivity. Together, with our analysis on the corresponding penetration depths, it is possible to make a purposeful decision on the selection of spatial frequency values.

There is a recent trend for experimental quantification of subdiffusive scattering and its associated parameter γ [14,17,27,28,35–38]. Based on our analytical computations, we contributed to the basic understanding of the significance and reliability of the γ parameter and demonstrated the potential absolute inaccuracy in γ to exceed 0.3, if the higher Legendre moments of the model scattering phase function are not considered properly. For absolute comparability of measured γ values, it is essential to make use of an appropriate scattering phase function model, which matches the basic angular scattering characteristics of the underlying sample. For biological tissue, fractal scattering might potentially serve as a good model, and we made the empirical finding that this model may be further approximated by the simpler modified powers of cosines function.

An important observation for phantom-based studies are the ambiguities in the γ reflectance relationship of a narrow size distribution of high refractive index scatterers. In such cases, it may not be possible to assign distinct γ values to the obtained reflectance intensities.

Funding. German Academic Exchange Service; Richard and Annemarie Wolf Foundation.

Acknowledgment. Support for this work has been provided by the Richard and Annemarie Wolf Foundation, Knittlingen, Germany, and by the German Academic Exchange Service through their provision of a DAAD postgraduate scholarship.

REFERENCES

1. D. J. Cuccia, F. Bevilacqua, A. J. Durkin, and B. J. Tromberg, "Modulated imaging: quantitative analysis and tomography of turbid media in the spatial-frequency domain," Opt. Lett. **30**, 1354–1356 (2005).
2. J. R. Weber, D. J. Cuccia, A. J. Durkin, and B. J. Tromberg, "Noncontact imaging of absorption and scattering in layered tissue using spatially modulated structured light," J. Appl. Phys. **105**, 102028 (2009).
3. D. J. Cuccia, F. Bevilacqua, A. J. Durkin, F. R. Ayers, and B. J. Tromberg, "Quantitation and mapping of tissue optical properties using modulated imaging," J. Biomed. Opt. **14**, 024012 (2009).
4. R. B. Saager, D. J. Cuccia, and A. J. Durkin, "Determination of optical properties of turbid media spanning visible and near-infrared regimes via spatially modulated quantitative spectroscopy," J. Biomed. Opt. **15**, 017012 (2010).
5. A. J. Lin, M. A. Koike, K. N. Green, J. G. Kim, A. Mazhar, T. B. Rice, F. M. LaFerla, and B. J. Tromberg, "Spatial frequency domain imaging of intrinsic optical property contrast in a mouse model of Alzheimer's disease," Ann. Biomed. Eng. **39**, 1349–1357 (2011).
6. D. Yudovsky and A. J. Durkin, "Spatial frequency domain spectroscopy of two layer media," J. Biomed. Opt. **16**, 107005 (2011).
7. A. M. Laughney, V. Krishnaswamy, E. J. Rizzo, M. C. Schwab, R. J. Barth, Jr, D. J. Cuccia, B. J. Tromberg, K. D. Paulsen, B. W. Pogue, and W. A. Wells, "Spectral discrimination of breast pathologies *in situ* using spatial frequency domain imaging," Breast Cancer Res. **15**, R61 (2013).
8. S. Gioux, A. Mazhar, D. J. Cuccia, A. J. Durkin, B. J. Tromberg, and J. V. Frangioni, "Three-dimensional surface profile intensity correction for spatially modulated imaging," J. Biomed. Opt. **14**, 034045 (2009).
9. A. Bassi, C. D'Andrea, G. Valentini, R. Cubeddu, and S. Arridge, "Detection of inhomogeneities in diffusive media using spatially modulated light," Opt. Lett. **34**, 2156–2158 (2009).
10. S. D. Konecky, A. Mazhar, D. Cuccia, A. J. Durkin, J. C. Schotland, and B. J. Tromberg, "Quantitative optical tomography of sub-surface heterogeneities using spatially modulated structured light," Opt. Express **17**, 14780–14790 (2009).
11. N. Bodenschatz, A. Brandes, A. Liemert, and A. Kienle, "Sources of errors in spatial frequency domain imaging of scattering media," J. Biomed. Opt. **19**, 071405 (2014).
12. S. L. Jacques, "Optical properties of biological tissues: a review," Phys. Med. Biol. **58**, R37–R61 (2013).
13. W.-F. Cheong, S. A. Prahl, and A. J. Welch, "A review of the optical properties of biological tissues," IEEE J. Quantum Electron. **26**, 2166–2185 (1990).
14. S. Chamot, E. Migacheva, O. Seydoux, P. Marquet, and C. Depeursinge, "Physical interpretation of the phase function related parameter γ studied with a fractal distribution of spherical scatterers," Opt. Express **18**, 23664–23675 (2010).
15. K. W. Calabro and I. J. Bigio, "Influence of the phase function in generalized diffuse reflectance models: review of current formalisms and novel observations," J. Biomed. Opt. **19**, 075005 (2014).
16. J. Wiest, N. Bodenschatz, A. Brandes, A. Liemert, and A. Kienle, "Polarization influence on reflectance measurements in the spatial frequency domain," Phys. Med. Biol. [posted 3 June 2015, in press].
17. S. C. Kanick, U. A. Gamm, H. J. C. M. Sterenborg, D. J. Robinson, and A. Amelink, "Method to quantitatively estimate wavelength-dependent scattering properties from multidiameter single fiber reflectance spectra measured in a turbid medium," Opt. Lett. **36**, 2997–2999 (2011).
18. F. Bevilacqua and C. Depeursinge, "Monte Carlo study of diffuse reflectance at source-detector separations close to one transport mean free path," J. Opt. Soc. Am. A **16**, 2935–2945 (1999).
19. A. Liemert and A. Kienle, "Spatially modulated light source obliquely incident on a semi-infinite scattering medium," Opt. Lett. **37**, 4158–4160 (2012).
20. A. Liemert and A. Kienle, "Exact and efficient solution of the radiative transport equation for the semi-infinite medium," Sci. Rep. **3**, 2018 (2013).
21. B. Gélébart, E. Tinet, J. M. Tualle, and S. Avrillier, "Phase function simulation in tissue phantoms: a fractal approach," Pure Appl. Opt. **5**, 377–388 (1996).
22. M. Xu and R. R. Alfano, "Fractal mechanisms of light scattering in biological tissue and cells," Opt. Lett. **30**, 3051–3053 (2005).
23. M. Xu, T. T. Wu, and J. Y. Qu, "Unified Mie and fractal scattering by cells and experimental study on application in optical characterization of cellular and subcellular structures," J. Biomed. Opt. **13**, 024015 (2008).
24. Y. Pu, W. Wang, M. AL-Rubaiee, S. K. Gayen, and M. Xu, "Determination of optical coefficients and fractal dimensional parameters of cancerous and normal prostate tissues," Appl. Spectrosc. **66**, 828–834 (2012).
25. J. M. Schmitt and G. Kumar, "Optical scattering properties of soft tissue: a discrete particle model," Appl. Opt. **37**, 2788–2797 (1998).

26. J. M. Schmitt and G. Kumar, "Turbulent nature of refractive-index variations in biological tissue," Opt. Lett. **21**, 1310–1312 (1996).
27. F. van Leeuwen-van Zaane, U. A. Gamm, P. B. A. A. van Driel, T. J. A. Snoeks, H. S. de Bruijn, A. van der Ploeg-van den Heuvel, I. M. Mol, C. W. G. M. Löwik, H. J. C. M. Sterenborg, A. Amelink, and D. J. Robinson, "*In vivo* quantification of the scattering properties of tissue using multi-diameter single fiber reflectance spectroscopy," Biomed. Opt. Express **4**, 696–708 (2013).
28. P. Thueler, I. Charvet, F. Bevilacqua, M. St. Ghislain, G. Ory, P. Marquet, P. Meda, B. Vermeulen, and C. Depeursinge, "*In vivo* endoscopic tissue diagnostics based on spectroscopic absorption, scattering, and phase function properties," J. Biomed. Opt. **8**, 495–503 (2003).
29. F. Bevilacqua, D. Piguet, P. Marquet, J. D. Gross, B. J. Tromberg, and C. Depeursinge, "*In vivo* local determination of tissue optical properties: applications to human brain," Appl. Opt. **38**, 4939–4950 (1999).
30. M. S. Patterson, S. Andersson-Engels, B. C. Wilson, and E. K. Osei, "Absorption spectroscopy in tissue-simulating materials: a theoretical and experimental study of photon paths," Appl. Opt. **34**, 22–30 (1995).
31. G. H. Weiss, R. Nossal, and R. F. Bonner, "Statistics of penetration depth of photons re-emitted from irradiated tissue," J. Mod. Opt. **36**, 349–359 (1989).
32. J. R. Mourant, J. Boyer, A. H. Hielscher, and I. J. Bigio, "Influence of the scattering phase function on light transport measurements in turbid media performed with small source-detector separations," Opt. Lett. **21**, 546–548 (1996).
33. G. J. Tearney, M. E. Brezinski, J. F. Southern, B. E. Bouma, M. R. Hee, and J. G. Fujimoto, "Determination of the refractive index of highly scattering human tissue by optical coherence tomography," Opt. Lett. **20**, 2258–2260 (1995).
34. K. Haseda, K. Kanematsu, K. Noguchi, H. Saito, N. Umeda, and Y. Ohta, "Significant correlation between refractive index and activity of mitochondria: single mitochondrion study," Biomed. Opt. Express **6**, 859–869 (2015).
35. S. C. Kanick, D. M. McClatchy III, V. Krishnaswamy, J. T. Elliott, K. D. Paulsen, and B. W. Pogue, "Sub-diffusive scattering parameter maps recovered using wide-field high-frequency structured light imaging," Biomed. Opt. Express **5**, 3376–3390 (2014).
36. D. M. McClatchy III, V. Krishnaswamy, S. C. Kanick, J. T. Elliot, W. A. Wells, R. J. Barth, Jr., K. D. Paulsen, and B. W. Pogue, "High spatial frequency structured light imaging for intraoperative breast tumor margin assessment," Proc. SPIE **9313**, 931308 (2015).
37. L. O. Reynolds and N. J. McCormick, "Approximate two-parameter phase function for light scattering," J. Opt. Soc. Am. **70**, 1206–1212 (1980).
38. I. Charvet, P. Thueler, B. Vermeulen, M. Saint-Ghislain, C. Biton, J. Jacquet, F. Bevilacqua, C. Depeursinge, and P. Meda, "A new optical method for the non-invasive detection of minimal tissue alterations," Phys. Med. Biol. **47**, 2095–2108 (2002).